Crystal Structure of the Actin Binding Domain of the Cyclase-Associated Protein†

Tetyana Dodatko,‡ Alexander A. Fedorov,‡ Marcin Grynberg,§,|| Yury Patskovsky,‡ Denise A. Rozwarski,‡ Lukasz Jaroszewski,§ Eliah Aronoff-Spencer,⊥ Elena Kondraskina,@ Tom Irving,@ Adam Godzik,§ and Steven C. Almo*,‡,⊥,#

Department of Biochemistry, Albert Einstein College of Medicine, Bronx, New York 10461, Department of Physiology and Biophysics, Albert Einstein College of Medicine, Bronx, New York 10461, Center for Synchrotron Biosciences, Albert Einstein College of Medicine, Bronx, New York 10461, Biophysics Collaborative Access Team, Advanced Photon Source, Argonne National Laboratory, Argonne, Illinois 60439, The Burnham Institute, La Jolla, California 92037, and Institute of Biochemistry and Biophysics, Polish Academy of Sciences, Warsaw, Poland

Received May 7, 2004; Revised Manuscript Received June 9, 2004

ABSTRACT: Cyclase-associated protein (CAP or Srv2p) is a modular actin monomer binding protein that directly regulates filament dynamics and has been implicated in a number of complex developmental and morphological processes, including mRNA localization and the establishment of cell polarity. The crystal structure of the C-terminal dimerization and actin monomer binding domain (C-CAP) reveals a highly unusual dimer, composed of monomers possessing six coils of right-handed β-helix flanked by antiparallel β-strands. Domain swapping, involving the last two strands of each monomer, results in the formation of an extended dimer with an extensive interface. This structural and biochemical characterization provides new insights into the organization and potential mechanistic properties of the multiprotein assemblies that integrate dynamic actin processes into the overall physiology of the cell. An unanticipated finding is that the unique tertiary structure of the C-CAP monomer provides a structural model for a wide range of molecules, including RP2 and cofactor C, proteins involved in X-linked *retinitis pigmentosa* and tubulin maturation, respectively, as well as several uncharacterized proteins that exhibit very diverse domain organizations. Thus, the unusual right-handed β-helical fold present in C-CAP appears to support a wide range of biological functions.

Dynamic remodeling of the actin cytoskeleton is essential for motility, cytokinesis, and a range of morphological and developmental programs. These processes rely on the coordination of signaling pathways that regulate the site and timing of filament (F-actin)[1] assembly, as well as the organization of individual filaments into higher-order structures. The cyclase-associated protein (CAP), also known as Srv2 in yeast, may provide one such linkage between the cytoskeleton and diverse signaling pathways. CAP was initially identified by biochemical and genetic approaches as a component of the RAS-responsive adenylate cyclase complex in budding yeast (*1*, *2*). A role for CAP in actin filament regulation was initially suggested by the observation that overexpression of profilin, a well-characterized actin monomer (G-actin) binding protein, suppressed the cytoskeletal defects associated with *cap*$^-$ cells (*3*).

Yeast CAP is a 526-residue tripartite modular protein (Figure 1). The amino-terminal domain (N-CAP, residues 1−168) binds to adenyl cyclase in yeast, supporting RAS-dependent stimulation of the cyclase (*4*, *5*), while in higher eukaryotes, the function of the N-terminus is unknown. The C-terminal domain (C-CAP, residues 370−526) binds G-actin with a 1:1 stoichiometry with an affinity in the range of 0.5−5.0 μM (*6*−*8*), and is responsible for oligomerization of the entire CAP molecule (*6*, *9*). Separating the N- and C-terminal domains is a proline-rich stretch that supports the binding of multiple SH3 domains, including the SH3 domain from abl, and ABP1 (actin binding protein 1), a 65 kDa modular F-actin binding protein that is thought to be responsible for localizing CAP (*6*, *10*). Two-hybrid data suggest a direct physical interaction between the N- and

† This work was supported by Grant GM53807 (S.C.A.). We acknowledge the *Dictyostelium* cDNA project in Japan, supported by the Japan Society for the Promotion of Science (RFTF96L00105) and the Ministry of Education, Science, Sports and Culture of Japan (08283107). Use of the Advanced Photon Source was supported by the U.S. Department of Energy, Basic Energy Sciences, Office of Science, under Contract W-31-109-ENG-38. BioCAT is a National Institutes of Health-supported Research Center (RR-08630). Data collection at the National Synchrotron Light Source was carried out on beamline X9B of the Albert Einstein Center for Synchrotron Biosciences, which is supported in part by a grant from the National Institute for Biomedical Imaging and Bioengineering (P41-EB-01979). Y.P. was supported by P50 GM62529 (S. K. Burley).

* To whom correspondence should be addressed: Department of Biochemistry, Albert Einstein College of Medicine, 1300 Morris Park Ave., Bronx, NY 10461. Phone: (718) 430-2746. Fax: (718) 430-8565. E-mail: almo@aecom.yu.edu.

‡ Department of Biochemistry, Albert Einstein College of Medicine.

§ The Burnham Institute.

|| Polish Academy of Sciences.

⊥ Department of Physiology and Biophysics, Albert Einstein College of Medicine.

@ Advanced Photon Source.

Center for Synchrotron Biosciences, Albert Einstein College of Medicine.

[1] Abbreviations: G-actin, monomeric actin; F-actin, filamentous actin; CAP, cyclase-associated protein; C-CAP, C-terminal domain of the cyclase-associated protein; N-CAP, N-terminal domain of the cyclase-associated protein; MAD, multiple anomalous dispersion; SAS, small-angle scattering; R_g, radius of gyration.

10.1021/bi049071r CCC: $27.50
Published on Web 07/30/2004

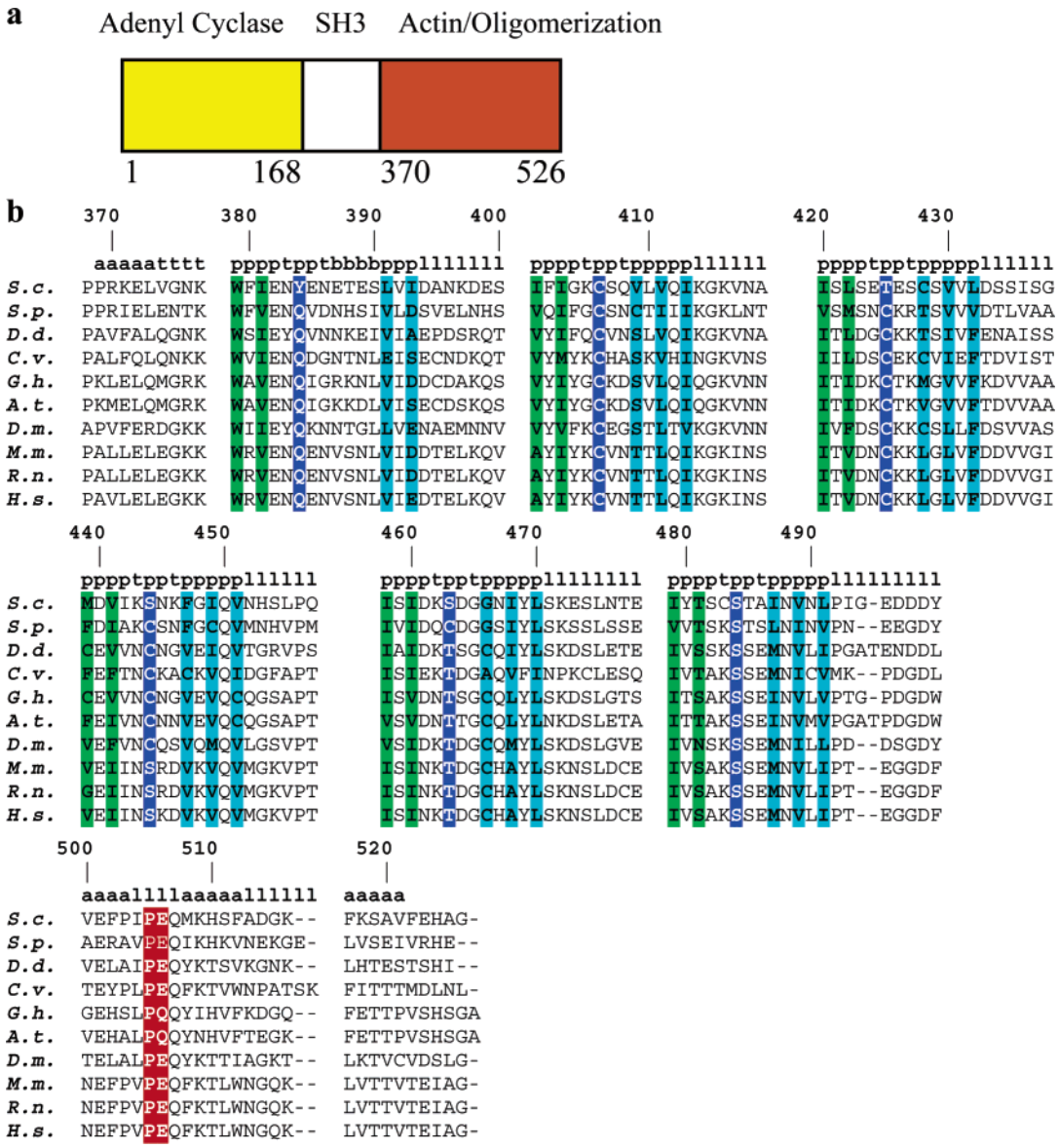

FIGURE 1: Modular organization of the cyclase-associated protein (CAP) and sequence alignment of the C-CAP domain. (a) Organization of the *S. cerevisiae* cyclase-associated protein (CAP) showing the domain boundaries for the functional modules. (b) Sequence alignment separated into modules. The central modules represent each turn of the right-handed β-helix. The lowercase letters above the amino acid sequence denote secondary structure elements (a, antiparallel β-strand; p, parallel β-strand; t, turn; b, β-strand bulge; l, loop). The buried residues of the a β-strands are shaded in green. The buried residues of the b β-strands are shaded in dark blue. The buried residues of the c β-strands are shaded in light blue. Pro505 and Glu506 of the extended C-terminal tail are shaded in red.

C-terminal domains of CAP, even though the functions of the N- and C-termini are not directly coupled (*9*). Interestingly, the N-terminal domain of CAP appears to regulate the ability of the proline-rich linker region to bind SH3 domains, and may therefore be involved in regulating subcellular localization via interaction with ABP1 (*11*). There is also some suggestion that the N-terminal domain may directly contribute to proper localization (*11*, *12*).

The amino acid sequence of CAP is highly conserved, and CAPs from a number of organisms are capable of complementing the *Saccharomyces cerevisiae* null, implying widespread conservation of CAP function (*13*−*16*) (Figure 1). CAP has been implicated in a number of developmental and morphological processes, including RNA localization and the establishment of cell polarity (*17*). Yeast lacking CAP show considerable variability in shape and size, suggesting a loss of polarization, likely due to defective vesicle targeting. In addition, the localization of specific mRNAs to the daughter bud is defective, perhaps due to a compromised cytoskeleton (*18*). In *Drosophila*, disruption of CAP results in a significant accumulation of filamentous actin and is associated with incorrect localization of specific mRNAs (*18*). Furthermore, during eye development in *Drosophila*, CAP defects lead to increased F-actin levels that are associated with alterations in cell morphology (*19*). Taken together, these observations in *Drosophila* suggest that the function of CAP is to limit the extent of actin polymerization. However, in mammalian cells, microinjection of CAP antibodies leads to a loss of stress fibers, while microinjection of CAP itself enhances stress fiber formation (*20*), suggesting that the role of CAP is to promote filament assembly. Recent biochemical studies suggest that CAP modulates filament turnover by regulating both barbed and pointed end dynamics (*21*).

Here we describe the crystal structures of yeast and human C-CAP at 2.3 and 2.8 Å resolution, respectively. The structure reveals a novel type of parallel right-handed β-helix,

which forms an intertwined dimer via exchange of a C-terminal β-hairpin. Competition assays with gelsolin, another G-actin binding protein, suggest that C-CAP binds in the proximity of subdomains 1 and 3 of actin. This unusual β-helical structure provides a template for modeling a wide range of biologically and clinically important molecules, including cofactor C, a component of the tubulin-specific chaperone system, and the gene responsible for X-linked *retinitis pigmentosa* (XRP2).

METHODS

Protein Preparation. The cDNA for the C-terminal domain of *S. cerevisiae* cyclase-associated protein (C-CAP, residues 369−526) was PCR amplified and subcloned into the *Nde*I−*Hin*dIII restriction sites of the pMW172 expression vector, which was used to transform *Escherichia coli* strain BL21-(DE3). Cells were grown for 18 h at 30 °C, without the addition of IPTG, and harvested by centrifugation at 10000*g*, and the cell pellet was resuspended in MEDA buffer at pH 7.0 (10 mM morpholinopropanesulfonic acid, 1 mM EGTA, 0.2 mM DTT, and 0.02% sodium azide) and lysed by the addition of lysozyme, followed by incubation on ice for 30 min and sonication. The lysate was centrifuged for 30 min at 16000*g*, and the supernatant was applied to a DE-52 column (Whatman, Madistone, U.K.) equilibrated with MEDA buffer. C-CAP was eluted with approximately 250 mM NaCl during the application of a linear gradient from 0 to 500 mM NaCl; appropriate column fractions were pooled, dialyzed against 4 M NaCl in MEDA buffer, and applied to a Phenyl-Sepharose CL-6B column (Amersham Pharmacia Biotech). C-CAP eluted at 0.6 M NaCl during the run of a linear gradient from 4 to 0 M NaCl; appropriate column fractions were pooled, dialyzed against MEDA buffer, and concentrated using Amicon Centriprep 10 concentrators. Selenomethionyl-substituted protein was expressed using the *E. coli* Met auxotroph B 834 (DE3) system after induction with 1 mM IPTG at 30 °C and purified as described for the native protein.

The C-terminal domain of human CAP1 (residues 319−475) was expressed in *E. coli* BL21(DE3)Lys STAR cells (Invitrogen) as a fusion to the full-length human GSTM2 containing a PreScission protease cleavage site (unpublished data). Cells were grown at 37 °C to an OD_{600} of 0.3, and expression was induced by the addition of 1.0 mM IPTG. Cells were grown for an additional 6 h at 37 °C, harvested by centrifugation (12000*g*), and resuspended in 50 mM Tris-HCl (pH 7.5), 0.15 M NaCl, 1 mM EDTA, and 1 mM DTT (loading buffer). Pancreatic DNase I (100 units/mL) was added to reduce viscosity. Cells were frozen at −70 °C and thawed at room temperature. The lysate was centrifuged for 30 min at 30000*g*, and the supernatant was applied to a glutathione−agarose (Sigma) column equilibrated with loading buffer. The column was washed with 20 volumes of wash buffer [50 mM Tris-HCl (pH 7.5) and 1.0 M NaCl] and then in 3 volumes of loading buffer. PreScission protease (Pharmacia) was added to the column (80 units/mL of beads), mixed with resin, and incubated overnight at 4 °C. Human C-CAP was eluted from the column using the same loading buffer, dialyzed against 20 mM Tris-HCl (pH 8.0), and concentrated as described above.

Full-length *Dictyostelium discoideum* cyclase-associated protein (Dicty-CAP) was PCR amplified and cloned into the *Bam*HI−*Sal*I restriction sites of the pGEX-6P-2 vector, which was used to transform *E. coli* BL(21)DE3. Cells were grown at 30 °C to an OD_{600} of 0.7−0.9, and expression was induced by the addition of 0.5 mM IPTG. Cells were grown for an additional 4−5 h at 20 °C, harvested by centrifugation (10000*g*), and resuspended in 50 mM Tris-HCl (pH 8.0), 150 mM NaCl, 1 mM EDTA, and 1 mM DTT (working buffer). Thereafter, 0.5 mM PMSF, $^1/_{10}$ volume of 10 mg/mL lysozyme (Sigma), and 130 units/mL DNase I were added. Cells were incubated on ice for 30 min and sonicated. The lysate was centrifuged for 45 min at 30000*g*, and the supernatant was incubated for 1−2 h at 4 °C with glutathione−Sepharose 4B equilibrated with the same buffer (2 mL of 50% slurry beads/L of culture). The resin was washed with at least 50 bed volumes of working buffer, followed by 10 volumes of cleavage buffer [50 mM Tris-HCl (pH 7.4), 150 mM NaCl, 1 mM DTT, and 1 mM EDTA]. CAP was released by cleavage with PreScission protease (80 units of protease/bed volume of GS matrix, 16 h at 4 °C) and eluted with cleavage buffer. CAP was further purified by gel filtration on Sephadex G-200 and concentrated.

Actin Binding Competition between Gelsolin and CAP. Protein samples were mixed, incubated at 4 °C for 1 h, and applied to 10 to 20% gradient Tris-HCl electrophoresis gels (Bio-Rad) under native conditions. The sample buffer contained 5% DTT (1 M), 0.06% bromophenol blue, and 10% glycerol. The running buffer consisted of 192 mM glycine and 25 mM Tris buffer. Gels were run for 6 h at 40 V and stained with Coomassie Blue.

S. cerevisiae C-CAP Crystallization. Crystals of *S. cerevisiae* C-CAP were produced by hanging drop vapor diffusion using a reservoir solution composed of 16% PEG 4000, 250 mM lithium sulfate, and 200 mM HEPES buffer (pH 7.6). Yeast C-CAP (10−20 mg/mL in MEDA buffer) was mixed with an equivalent volume of reservoir solution, and equilibrated over 1 mL of reservoir solution. Crystals with a tetragonal bipyramidal morphology and a maximum dimension of 0.3 mm on their longest axis appeared within several days. Before being flash-cooled to −170 °C, yeast C-CAP crystals were transferred to a cryoprotectant composed of mother liquor supplemented with 15% glycerol. These crystals diffracted X-rays to 2.3 Å resolution under cryogenic conditions at beamline X9B at the National Synchrotron Light Source (Brookhaven National Laboratory, Upton, NY). Diffraction from these crystals is consistent with either orthorhombic space group $I222$ or $I2_12_12_1$ [$a = 56.52$ Å, $b = 86.81$ Å, and $c = 160.21$ Å; two molecules in the asymmetric unit (Matthews coefficient of 3.4 and 64% solvent content)].

Crystallographic Data Collection, Phasing, and Model Refinement. A self-rotation function using POLARRFN (*22*) revealed the orientation of a noncrystallographic symmetry (NCS) 2-fold axis (CCP4 convention, $\phi = 270.5°$, $\psi = 45.0°$, $\kappa = 180.0°$; XPLOR convention, $\phi = 90.5°$, $\psi = 45.0°$, $\kappa = 180.0°$). A three-wavelength MAD data set was collected (inflection = 0.9790 Å, edge = 0.9788 Å, and remote = 0.9416 Å) using inverse beam geometry at −170 °C with a Quantum4 CCD detector (Area Detector Systems Corp., Poway, CA). The raw diffraction data were processed with the HKL suite of programs (*23*) (Table 1). The locations of the two selenium atoms per C-CAP subunit (totaling four

Table 1: *S. cerevisiae* C-CAP Structure Solution

3.0 Å Seleno-Met MAD Data[a]

	inflection, λ_1 (maximized for dispersive signal)	edge, λ_2 (maximized for anomalous signal)	remote, λ_3 (pseudo-native)
wavelength	0.9790	0.9788	0.9416
no. of observations	46479	47915	49025
no. of unique reflections	13671	13742	13840
completeness (%)	90.0	90.4	91.1
average $I/\sigma I$	18.9	18.8	18.6
R_{sym}	0.058	0.054	0.052

differences	λ_1	λ_2	λ_3	f'	f''
λ_1	0.050	0.026	0.042	−8.3	2.2
λ_2		0.056	0.033	−8.1	3.8
λ_3			0.044	−2.3	3.5

High-Resolution (2.3 Å) Native Data[b]

	last shell (2.38−2.30 Å)	overall (10.00−2.30 Å)
no. of observations	7805	105428
no. of unique reflections	1564	17479
completeness (%)	91.1	97.3
average $I/\sigma I$	18.1	49.7
R_{sym}	0.100	0.038
R	0.224	0.207
R_{free}	0.279	0.242

	no. of non-hydrogen atoms	average temperature factor
protein main chain	1240	25.5
protein side chain	1166	28.5
ordered water molecules	160	39.4
total	2576	27.6

[a] Statistics from SOLVE: mean figure of merit = 0.44; overall quality of solution = 33.9. Statistics after solvent flattening: mean figure or merit = 0.69. [b] rms deviations from ideal geometry: 0.006 Å for bond lengths, 1.23° for bond angles, 27.60° for dihedral angles, and 0.63° for improper angles.

per asymmetric unit) were determined with SOLVE (*24*) (confirming the space group as $I2_12_12_1$). The locations of the selenium atom sites displayed the previously determined NCS 2-fold symmetry.

Phases and electron density maps were calculated with SOLVE, and the map was improved by solvent flattening using DM (*22*). Utilizing methionine residues 439 and 508 as fiducial markers, the entire C-CAP sequence (155 consecutive residues) was manually fit to the 3.0 Å resolution solvent-flattened MAD map. The MAD map (Figure 2) was of sufficient quality that 2-fold NCS averaging did not produce significant improvement.

Higher-resolution native data (2.3 Å) were collected with native crystals at a low temperature (−170 °C) using synchrotron radiation (wavelength = 1.04 Å) coupled to a MAR345 image plate detector on beamline X9B at Brookhaven National Laboratory (Table 1). Refinement was performed with XPLOR and CNS (*25*), and included NCS restraints, including several rounds of simulated annealing refinement, conventional positional refinement, individual temperature factor refinement, and manual model building. Additional rounds of adjustments to the protein model, and incorporation of 160 ordered water molecules, followed by conventional positional refinement, individual temperature factor refinement, and overall anisotropic temperature factor refinement were performed ($R = 0.207$, $R_{free} = 0.242$). The coordinates have been deposited in the Protein Data Bank as entry 1K4Z. Secondary structure assignment was based on the Kabsch−Sander algorithm [PROCHECK (*26*)], but with the extra criteria that all residues must have the appropriate (ϕ and ψ) angles as well as being hydrogen bonded.

Crystallization and Data Collection for the Human C-CAP Structure. Crystals of human C-CAP were grown at 16 °C by sitting drop vapor diffusion in the presence of 0.1 M Tris-HCl (pH 8.5), 27.5% PEG 4000, 0.2 M sodium acetate, and a protein concentration of 12−24 mg/mL. Tetragonal rod-shaped crystals reached a maximal length of ∼1 mm and a width of 0.2 mm in 4−7 days. For data collection, crystals were frozen in liquid nitrogen after being soaked in mother liquor supplemented with 15% glycerol as a cryoprotectant. X-ray data were collected to 2.8 Å resolution under cryogenic conditions using a Rigaku RU-200 X-ray generator coupled to a RIGAKU R-AXIS IV image plate. Data were reduced and scaled with DENZO and SCALEPACK, yielding an overall completeness of 95% and an R_{merge} value of 5.9%. The unit cell dimensions were as follows: $a = 82.64$ Å, $b = 83.12$ Å, and $c = 99.96$ Å (with a pattern of systematic absences consistent with a $P2_1\ 2_1\ 2_1$ space group).

Molecular Replacement and Refinement of the Human C-CAP Structure. Molecular replacement was carried out using the strand-exchanged yeast C-CAP dimer as the search model and X-PLOR (version 3.851). The cross-rotation function, followed by PC refinement protocols, using data in the 15.0−4.0 Å resolution range, yielded two clear solutions corresponding to separate homodimers in the asymmetric unit. A subsequent translation function search and rigid-body refinement produced a model with an initial R_{free} of 0.52 and an R of 0.47. At this point, the yeast sequence was replaced with that of human C-CAP, and multiple rounds of refinement using strict NCS values yielded R and R_{free} values of 0.24 and 0.28, respectively. Manual adjustment of the model and additional rounds of refinement, using 15 935 reflections (σ/F cutoff = 2.0) in the 10.0−2.8 Å resolution range, yielded a final model with R and R_{free} values of 0.232 and 0.268, respectively, with rms deviations for bonds of 0.005 Å, for bond angles of 1.34°, and for improper angles of 0.64° (Table 2). The quality of the final model was verified by PROCHECK (*26*), and all residues are within allowed regions of the Ramachandran plot with 81% in the most favorable regions.

Small-Angle X-ray Scattering. SAS experiments were conducted on Biophysics Collaborative Access Team (BioCAT) undulator beamline 18-ID at the Advanced Photon Source. Samples were exposed to focused X-rays (12 000 ± 20 eV, $\sim 1 \times 10^{12}$ photons/s) for 12.2 s, using a specimen−detector distance of 2.78 m. Two-dimensional scattering patterns were obtained using a 5 cm × 9 cm CCD detector (*60*). For exposure, a 100 μL sample was contained in a 1.5 mm diameter borosilicate glass capillary and oscillated at 4 μL/s using a programmable syringe pump (Hamilton model 541C) to control radiation damage. Scattering over a range of q from 0.004 to 0.13 Å^{-1} was calculated from radial integrations of the two-dimensional scattering patterns using the routines in the FIT2D data analysis program (Hammersley 1998, Fit2D version 9.129

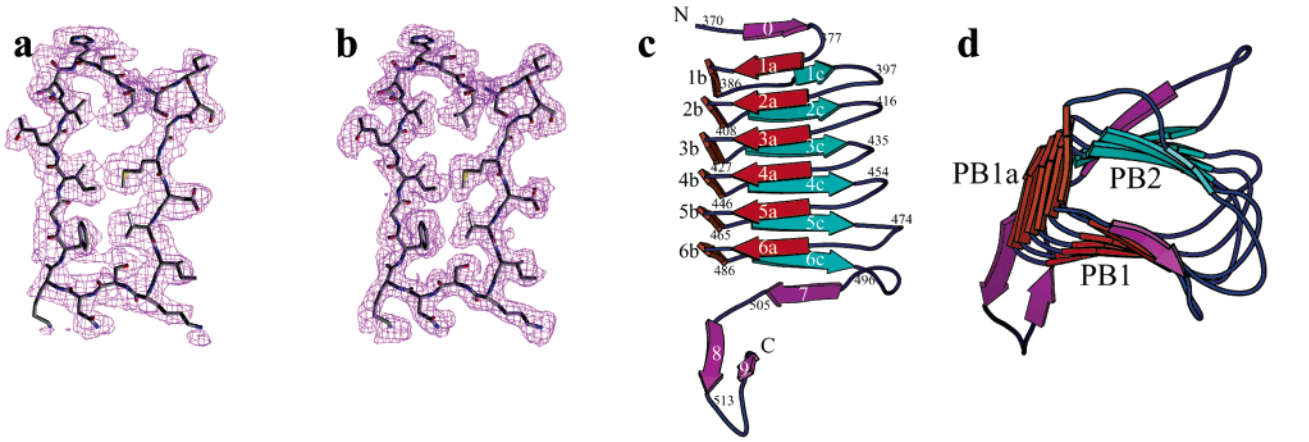

FIGURE 2: Structure of the *S. cerevisiae* cyclase-associated protein C-terminal domain (C-CAP). (a) The 3.0 Å experimental electron density for a single coil of the *S. cerevisiae* C-CAP calculated from a three-wavelength selenomethionyl MAD experiment (contoured at 1σ). The final refined model is superimposed. (b) The final $2F_o - F_c$ map calculated at 2.3 Å (contoured at 1σ) with the final model superimposed. (c) Ribbon diagram of the C-CAP monomer viewed perpendicular to the β-helical axis. Each of the 22 β-strands is labeled according to its position within or outside the β-helical core region; residue numbers serve as markers that denote the direction of the polypeptide chain. (d) C-CAP monomer viewed down the β-helical axis; the three parallel β-sheets are denoted PB1, PB1a, and PB2.

Table 2: Human C-CAP Structure Solution[a]

	last shell (2.92−2.80 Å)	overall (10.00−2.80 Å)
no. of observations	10337	151537
no. of unique reflections	1846	15935
completeness (%)	90.5	93.3
average $I/\sigma I$	6.3	20.2
R_{sym}	0.154	0.054
R	0.292	0.232
R_{free}	0.327	0.268

[a] The average temperature factor for all protein atoms = 26.6; rms deviations from ideal geometry: 0.005 Å for bond lengths, 1.34° for bond angles, 31.45° for dihedral angles, and 0.64° for improper angles.

Reference Manual, ESRF Internal Report ESRF98HA01T). Integrated scattering profiles from sample with buffer and buffer alone were scaled using incident flux values integrated over the exposure time. The experimental radius of gyration (R_g) was calculated conventionally as the square root of −3 times the slope from plots of ln(I) versus q^2, where I is the difference in intensity in scattering patterns from the sample in buffer minus the buffer alone. R_g of the crystallographic model was calculated as $(\sum_i m_i r_i^2/\sum_i m_i)^{1/2}$, where r_i is the distance between each mass element (m_i) and the center of mass.

RESULTS

Structure of S. cerevisiae C-CAP. The structure of *S. cerevisiae* C-CAP was determined by multiple anomalous dispersion (MAD) using selenomethionyl-substituted protein and 2-fold noncrystallographic symmetry averaging (Figure 2 and Table 1). The central core of the C-CAP monomer is composed of six coils of right-handed parallel β-helix, termed coils 1−6, which form an elliptical barrel (major axis, 22 Å; minor axis, 10 Å; based on α-carbons) with a tightly packed interior (Figures 2 and 3). Each β-helical coil is composed of three relatively short β-strands, designated a−c, separated by sharp turns (Figure 3). If on adopts the nomenclature utilized for pectate lyase (*27, 28*), the archetypal β-helical structure, the a−c strands form three parallel β-sheets that are denoted PB1, PB1a, and PB2, respectively. The individual strands are designated by their order of appearance within a given coil (i.e., the third strand in the fourth coil is identified as c4). Flanking the central β-helical core is an N-terminal β-strand, β0, that packs antiparallel to the core, and strand β7 packs antiparallel to the core near the C-terminal end of the parallel β-helix. The resultant mixed β-sheets, β0a1a2a3a4a5a6 and c1c2c3c4c5c6β7, are extensions of sheets PB1 and PB2, respectively, of the parallel β-helical core. The C-CAP monomer also contains a remote β-hairpin, composed of antiparallel β-strands β8β9, which extends away from the β-helical core (Figure 2).

PB1 and PB2 in C-CAP are structurally equivalent to PB1 and PB2, respectively, of pectate lyase (Figures 2 and 3), while the equivalent of PB1a is absent in pectate lyase. The C-CAP β-helix exhibits considerable regularity, as the β-strands in sheet PB1 contain four to five residues, all strands in PB1a are composed of two residues, and the strands in PB2 are composed of four to six residues. Individual strands in PB2 are connected to PB1 of a subsequent coil of the β-helix by a loop that ranges from four to six residues in length. The three individual β-strands within a coil are separated by a single residue that adopts a left-handed α-helical (α_L) conformation. These α_L residues have a dramatic effect on local structure as they result in a 90° alteration in the main chain direction. The number of residues in a single β-helical turn in C-CAP varies from 19 to 22, with an average of 20 residues in a complete turn, and a mean separation of 4.9 Å between adjacent coils. This organization results in an average rise per residue of 0.24 Å, which closely approximates a perfect circular parallel β-helix with 22 residues per turn and a 0.22 Å rise per residue. The six β-helical turns in C-CAP superimpose with a root-mean-square displacement of 1.2 Å for equivalent α-carbon positions (excluding residues in the loop regions), highlighting the regularity of the core structure.

Stabilization of the C-CAP Fold. The C-CAP β-helix is supported by the near-ideal interstrand main chain hydrogen bonds, within the PB1, PB1a, and PB2 parallel β-sheets, which are oriented parallel to the β-helical axis. This arrangement directs the side chains of alternate residues within the strands toward either the solvent or the hydrophobic core of the molecule (Figure 3). Significant main

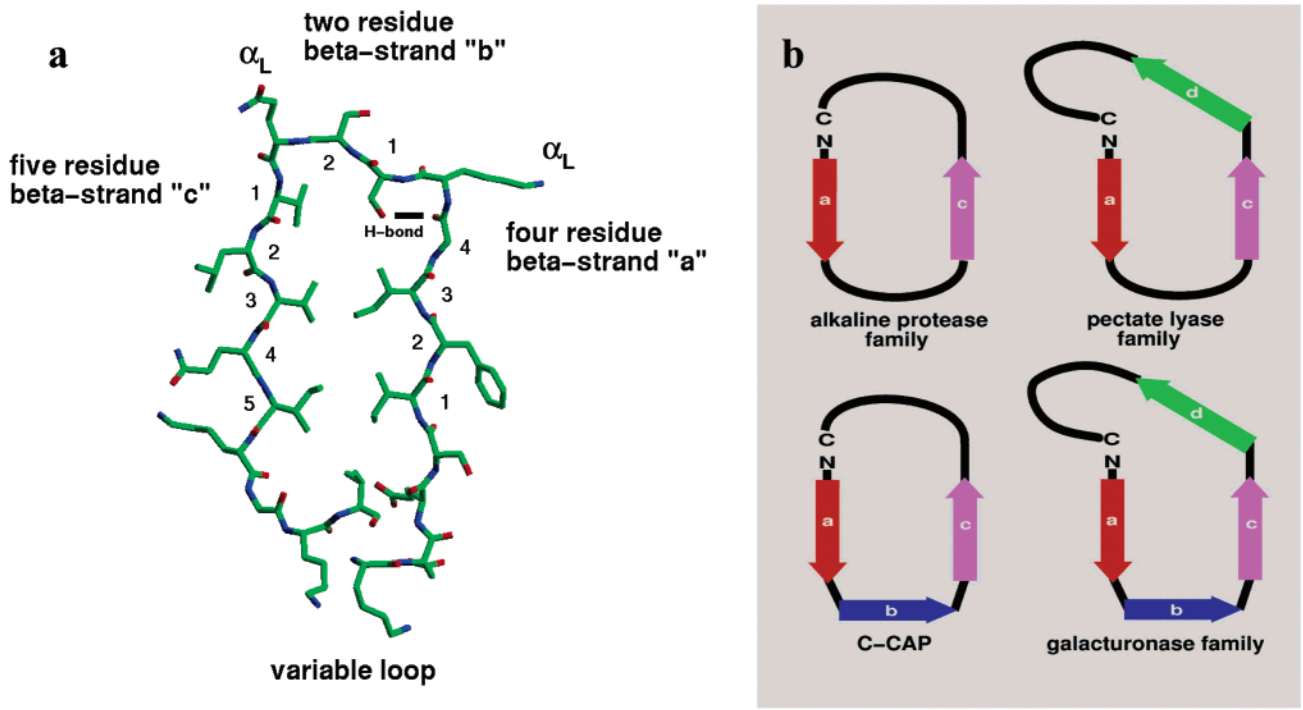

FIGURE 3: Features of the right-handed β-helix family. (a) Arrangement of residues in a β-helical turn of C-CAP. Each β-helical turn contains a four- or five-residue β-strand (labeled a) that contributes to sheet P1, a two-residue β-strand (labeled b) that contributes to sheet P1a, a four- to six-residue β-strand (labeled c) that contributes to sheet P2, and a variable loop connecting turns of subsequent layers. Within individual turns of the β-helical core, strands are separated by single residues in the α_L conformation. For every turn, the first residue of the b β-strands contains a hydrophilic side chain (Ser, Thr, or Cys) that hydrogen bonds to the carbonyl oxygen of the fourth residue of the a β-strands. The second coil of the β-helix is displayed. (b) Comparison of the backbone topology of one β-helical turn among different right-handed β-helical families demonstrates that the shape of the C-CAP cylindrical shaft is unique. The members of the alkaline protease family (for example, PDB entries 1kap and 1sat) contain two β-strands per β-helical turn, labeled a and c. The members of the pectate lyase family (for example, PDB entries 2pec and 1idk) contain three β-strands per β-helical turn as a consequence of the addition of β-strand d. C-CAP also contains three β-strands per β-helical turn as a consequence of the addition of the topologically distinct β-strand b. The members of the galacturonase family (for example, PDB entries 1rmg and 1bne) contains four β-strands per β-helical turn, by the addition of β-strands both b and d.

chain hydrogen bonding interactions are also present between the loop segments that join adjacent coils in the β-helix. Two such hydrogen bonds connect coils 1 and 2, coils 2 and 3, and coils 3 and 4, while coils 4 and 5 are connected by three main chain hydrogen bonds between the respective loop segments. The hydrophobic core of the C-CAP β-helix is formed by the packing of the PB1 and PB2 sheets against each other. These sheets contribute small aliphatic side chains, predominately Val, Leu, and Ile, such that the distance between equivalent α-carbon atoms of these two sheets is ~10 Å. When viewed down the axis of the parallel β-helix, the side chains of PB1 and PB2 appear to abut each other; however, when viewed perpendicular to the axis of the β-helix, the side chains of both sheets are interdigitated with each other.

The β-helix exhibits an extraordinary alignment of hydrophobic and hydrophilic side chains both in the interior and on the surface of the molecule. This arrangement is a consequence of the interstrand main chain hydrogen bonding interactions that align β-carbon atoms from adjacent β-strands above each other. Within the core of the yeast C-CAP β-helix, this registration results in the formation of extensive stacks of small aliphatic side chains, including Ile381-Ile403-Leu422-Val441-Ile460, Ile401-Ile420, Ile458-Ile479, Leu391-Val411-Val430-Ile449-Ile468-Val489, and Ile393-Ile413-Leu432-Val451-Leu470-Leu491. Of particular note is the interior stack of Cys406-Thr425-Ser444-Ser463-Ser484 hydrophilic residues. All of these polar residues are located in the first position of the b strands that form the PB1a sheet and are accommodated by specific hydrogen bonding interactions. Cys406 and all three serine residues donate hydrogen bonds to the main chain carbonyl oxygen of residue $i - 2$, which is the last residue in the a strands that form the PB1 sheet. Careful examination of the electron density corresponding to Thr425 reveals a side chain rotamer conformation that does not support interaction with the carbonyl oxygen of residue 423 but, instead, suggests hydrogen bonding interactions with side chain of Ser444 in the adjacent coil. Notably, in all CAP sequences, the identity of the first residue in strand b within coils 2−6 is restricted to Ser, Thr, or Cys, indicating that the detailed hydrogen pattern observed in the yeast protein is a general feature of the entire CAP family. This structural motif of stacked, buried hydrophilic residues along one side of the cylindrical shaft is also well-documented in other β-helical structures (*28*, *29*).

Several other polar side chains, including those of Cys428, Ser435, Ser474, Thr477, and Asn490, are buried to an extent of ≥95%, and are accommodated in the hydrophobic core by interactions with main chain carbonyls or side chain hydroxyls. Two water molecules are buried inside the hydrophobic core of the C-CAP β-helix. The first water is hydrogen bonded to main chain Gly415 O, Asp433 N, and Ser434 O atoms, and connects two adjacent coils of the β-helix. The second internal water is hydrogen bonded to main chain Cys428 N and Asn445 O atoms and the side

chain of Thr425. Both of these internal water molecules are independently observed in the two NCS-related C-CAP molecules.

The antiparallel elements that flank the parallel β-helical core are a consequence of specific interactions. The tight two-residue turn that promotes the antiparallel disposition of strands β0 and a1 contains the highly conserved Gly376, which adopts an unusual backbone conformation ($\phi = 73.3°$ and $\psi = -113°$) required to accommodate this chain reversal. This antiparallel topology is supported by an ionic interaction between Arg371 and Glu382 in strands β0 and a1, respectively. At the C-terminus of the β-helical core, a second chain reversal directs the antiparallel interaction between strands c6 and β7. This change in main chain direction begins at the nearly invariant Pro492 and continues into a loose six-residue turn. In the yeast protein, this chain reversal is stabilized by a "herringbone" aromatic−aromatic interaction between Tyr469 and Tyr499, and possibly by an ionic interaction between Lys472 and Asp497 that connects strand 5c with the loop between strands 6c and β7. As described below, this chain reversal is functionally significant as it allows β8β9 to be situated distal to the β-helical core and thus indirectly supports the formation of the physiological dimeric species.

C-CAP NCS Dimer Structure. The asymmetric unit of the yeast C-CAP crystals contains two molecules, related by proper 2-fold noncrystallographic (NCS) symmetry (Figure 4). The β-helical axes of the two monomers are antiparallel to each other and perpendicular to the NCS 2-fold axis. This interface buries 934 Å^2 of total accessible surface area and is stabilized by three direct polar interactions [Asn418 OD1−Asn418′ ND2, Ser437 O−Asn37′ ND2, and Ser437 O−Lys378′ NZ (the prime denotes contributions from the symmetry-related molecule)], as well as additional water-mediated hydrogen bonds. No hydrophobic interactions are observed between the two NCS monomers. The two NCS-related monomers are very similar, as all 157 α-carbon pairs superimpose with an rms deviation of 0.28 Å, with only the loop segment composed of residues 493−498 exhibiting substantially different conformations in two NCS-related monomers due to lattice contacts.

C-CAP Strand-Exchanged Dimer Structure. Two crystallographically related C-CAP monomers exchange their remote β-hairpins (antiparallel strands β8β9), resulting in an intimate "strand-exchanged dimer" that buries a total accessible surface area of 2558 Å^2 (Figure 4). When viewed perpendicular to the crystallographic 2-fold axis, the dimer resembles the letter V. The front and backsides of the V-shaped molecules are composed of seven-stranded and nine-stranded β-sheets, respectively, with the cavity being bounded by the symmetry-related PB1a β-sheets, and the external sides formed by six parallel loops on each monomer. Viewed down the crystallographic 2-fold axis, this intertwined dimer exhibits a serpentine or S-shaped organization, with 2-fold symmetry-related concave and convex surfaces. The concave surfaces are composed of nine-stranded mixed β-sheets formed by the β0a1a2a3a4a5a6β8′β9′ strands, and the convex surfaces are composed of the seven-stranded mixed β-sheets containing the c1c2c3c4c5c6β7 strands.

The formation of the strand-exchanged dimer is a consequence of the polypeptide segment (residues 505−508) connecting β-strands β7 and β8, which adopts an extended conformation and results in the placement of the β8β9 hairpin distal to the core of the β-helix. This placement allows β8 to participate in extensive antiparallel hydrogen bonding interactions with strand a6′ in the PB1 sheet of the symmetry-related monomer. In addition to the a6β8′ and a6′β8 main chain hydrogen bonds, the strand-exchanged dimer is further stabilized by the contribution of 13 predominately hydrophobic residues from each 2-fold related monomer (Leu475, Ile479, Val489, Leu491, Ile493, Phe502, Ile504, Pro505, Met508, His510, Phe512, Phe517, and Val521). The β8β9 hairpin and its symmetry mate cross at the crystallographic 2-fold axis, which is centered on Glu506 and Gln507 and Glu506′ and Gln507′ of the exchanged strands. The exchanged strands do not participate in β-sheetlike main chain hydrogen bonds in this central crossover region. The exchanging strands participate in hydrophobic interactions involving Ile504−His510′, Pro505−Met508′, and their symmetry mates, and Met508−Met508′. Several main chain−side chain hydrogen bonding interactions may also contribute to the stability of the dimer. The side chain of Glu506 interacts with the main chain amide nitrogen of Ala486′ in the sixth coil of the β-helix, and the Gln507 side chain forms water-mediated hydrogen bonds with Ile460′ O and Tyr480′ O contributed by the fifth and sixth coils of the symmetry-related molecule, respectively. Consistent with the roles of residues 505−507 in stabilizing the strand-exchanged dimer, Pro505 is absolutely conserved in all known species; position 506 allows the conservative substitution of only glutamate or glutamine, and with only a single exception, Gln507 is invariant.

The PB1a β-sheets exhibit only a single interaction in the 2.3 Å yeast structure, a disulfide bridge formed by Cys483 and Cys483′. However, given the cytoplasmic disposition of CAP and the presence of a Lys at this position in all other members of the CAP family, this is not likely to be a physiologically relevant disulfide linkage. Furthermore, this disulfide is not observed in other structures (data not shown), indicating that the observed disulfide is an artifact resulting from oxidation after crystallization. The artificial nature of the observed disulfide is also consistent with the behavior of freshly prepared material on reducing and nonreducing SDS−PAGE (data not shown).

Validation of the C-CAP Dimer. As the strand-exchanged yeast C-CAP exhibits a rather unusual dimer interface, we sought independent confirmation. Small-angle X-ray scattering data are fully consistent with the strand-exchanged dimer, as the experimentally determined radius of gyration ($R_g = 24.2$ Å) compares favorably with that calculated from the yeast C-CAP dimer structure (24.1 Å) (Figure 5).

Further validation of the strand-exchanged dimer was provided by the structure of human C-CAP, which was determined by molecular replacement and refined to 2.8 Å resolution (Table 2). Crystals of human C-CAP contain four monomers in the asymmetric unit, which form two dimers displaying the same quaternary organization observed for the strand-exchanged yeast dimer. The two strand-exchanged human C-CAP dimers superimpose with an rms deviation of 0.6 Å for all atoms, and like the yeast dimer buries ~2600 Å^2 of solvent accessible surface area. The human and yeast C-CAP also exhibit extensive detailed similarity, as the monomers and dimers superimposed with rms deviations of 0.9 and 1.2 Å between backbone atoms, respectively (Figure

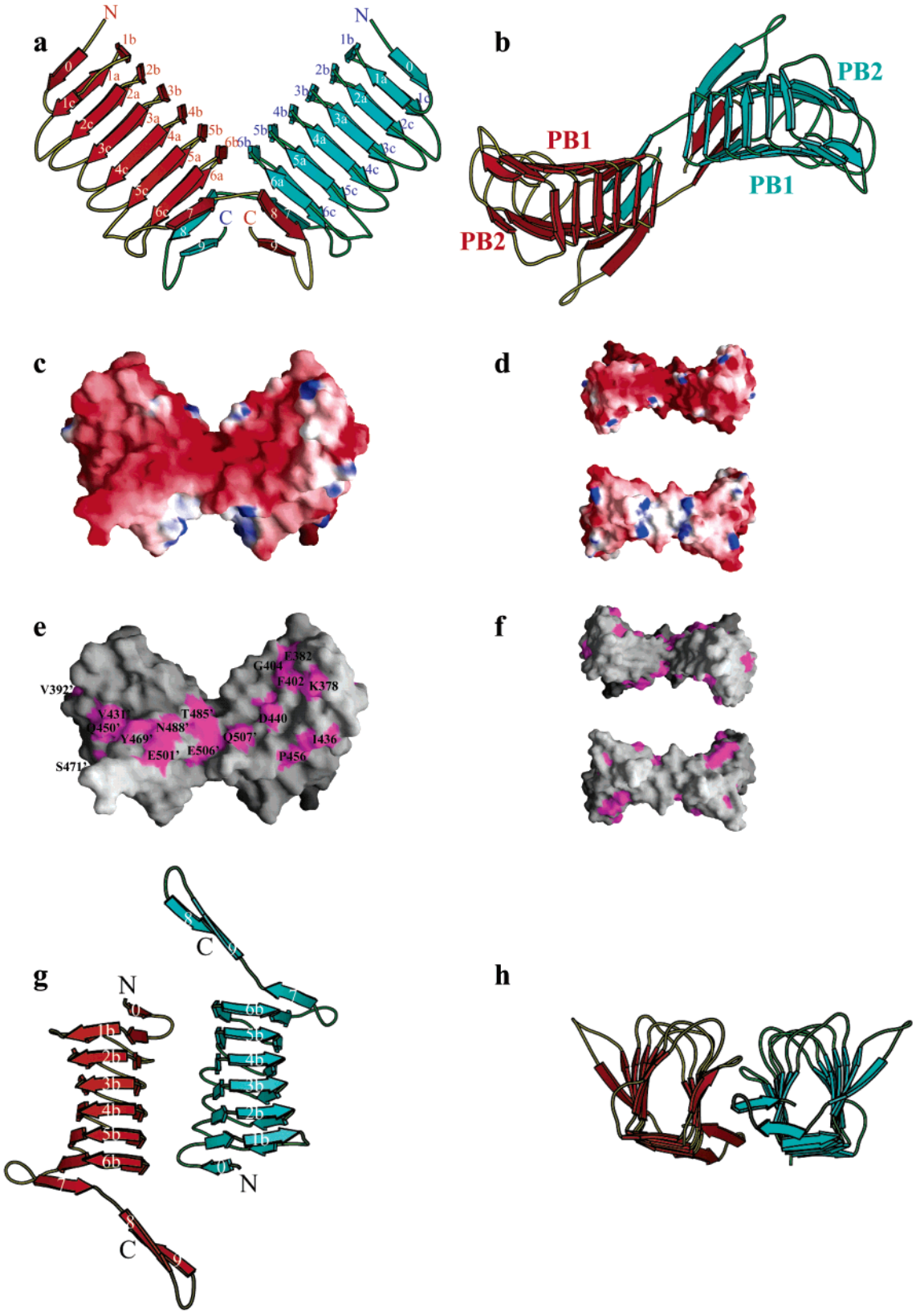

FIGURE 4: Structural and functional features of C-CAP dimers. (a) Physiological C-CAP dimer viewed perpendicular to the 2-fold dimer axis. This dimer is formed by the exchange of the last two strands of each monomer. (b) Physiological C-CAP dimer viewed down the dimer axis. (c) Electrostatic surface potential of the yeast C-CAP viewed perpendicular to the molecular 2-fold axis, contoured at $\pm 10kT/e^{-}$. The positive potential is blue, and the negative potential is red. (d) Electrostatic surface potential viewed parallel to the molecular 2-fold axis. The top and bottom parts of the panel display the top and bottom, respectively, of the C-CAP domain with respect to panel c. (e) Mapping of conserved surface accessible residues viewed perpendicular to the 2-fold axis. (f) Conserved surface accessible residues viewed parallel to the molecular 2-fold axis as in panel d. (g) Noncrystallographic (NSC) dimer viewed down the NCS axis. (h) View of the NCS dimer perpendicular to the NCS axis.

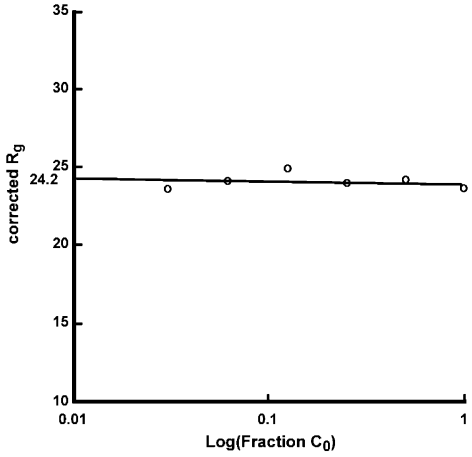

FIGURE 5: Validation of the C-CAP dimer by small-angle X-ray scattering. The experimentally determined radius of gyration (R_g = 24.2 Å) compares favorably with that calculated from the strand-exchanged extended yeast C-CAP dimer structure (24.1 Å).

6). In total, these findings support the validity of the observed strand-exchanged dimer and suggest that this C-CAP quaternary organization is conserved throughout evolution.

Biochemical Assessment of the C-CAP−Actin Interaction. Native gel analysis was used to perform competition assays to map the C-CAP binding surface on the actin monomer. Gelsolin segment-1 (S1), a well-characterized actin binding module, has been shown by direct crystallographic observation to bind a hydrophobic cleft formed by subdomains 1 and 3 on the actin monomer (*30*). Figure 7 demonstrates that CAP and S1 compete for binding to G-actin. The most parsimonious interpretation is that C-CAP contacts a surface in the proximity of subdomains 1 and 3, which is similar to or overlaps with the S1 binding site (Figure 7). This interpretation is also consistent with the observation that the C-CAP−G-actin complex interacts with DNase I, which binds tightly to subdomain 2 of G-actin.

Homology Modeling. With the sequence of yeast C-CAP as the starting point, a cascade of PSI-BLAST (*31*) searches was performed using the Saturated-BLAST protocol (*32*). An *e*-value threshold of $e - 5$ was used for the automatic acceptance of new members of the family, and below-threshold similarities were accepted only if verified by FFAS (*33*), a sensitive profile−profile comparison algorithm (*32*).

DISCUSSION

Implications for CAP Function. Several models have been proposed for the organization of the CAP dimer (*34*). The work presented here convincingly supports a parallel dimer, involving domain swapping in the C-terminal domain, which is consistent with the tripartite domain organization of the full-length cyclase-associated protein. The disposition of the amino termini in the strand-exchanged dimer would direct the beginning of the proline-rich domain away form the β-helical core, running nearly orthogonal to the β-helical axis. The considerable conformational plasticity likely associated with this low-complexity segment may allow N-CAP to physically contact C-CAP, and would be consistent with yeast two-hybrid data showing an interaction between the two domains (*9*); however, these observations cannot distinguish whether the interaction between these two domains is inter- or intramolecular.

Yeast two-hybrid analysis also suggested that the actin binding surface of the cyclase-associated protein includes residues 499−526, located at the extreme C-terminus of the protein, as deletion of these residues results in the loss of the observed interaction (*9*). On the basis of this structure, this interpretation must be carefully reconsidered, as these same residues direct the formation of the strand-exchanged CAP dimer, and are responsible for "capping" the hydrophobic interior of the β-helical core. Thus, the loss of actin binding activity in the two-hybrid assay may be the consequence of a structurally compromised CAP molecule, and not due to direct disruption of the actin binding surface.

Further functional insights may be gleaned from the physical properties and distribution of solvent accessible amino acids. The concave (i.e., the β0a1a2a3a4a5a6β8′β9′ sheet) and convex (i.e., the c1c2c3c4c5c6β7 sheet) surfaces that form the sides of the dimer are characterized by the presence of a considerable number of acidic groups as judged by an examination of the electrostatic potential (Figure 4c). Likewise, the top of the strand-exchanged dimer also exhibits a clustering of anionic groups, while the bottom of the dimer appears to be considerably less ionic in nature, with contributions of only a few basic groups (Figure 4d). Several highly conserved residues, including Val431, Gln450, Tyr469, Thr485, Asn488, Glu501, Glu506, and Gln507, form a semicontinuous patch on the convex surface, while the concave surface has a somewhat more punctate distribution of highly conserved residues, including Lys378, Glu382, Phe402, Ile436, Asp440, and Pro456 (Figure 4e,f). While it is likely that these conserved patches represent binding surfaces for interacting proteins (or domains), existing data do not allow the identification of G-actin or N-CAP binding sites.

The C-CAP structure also provides some insight into the organization of the multicomponent assemblies that may contribute to the formation and regulation of filamentous actin assemblies *in vivo*. The relative placement of the conserved surface features with respect to the molecular-2-fold axis of the strand-exchanged dimer would allow each monomer to bind an independent actin monomer, and is consistent with biochemical studies demonstrating that CAP associates with actin in a 1:1 (monomer:monomer) stoichiometric complex (*6*−*8*, *35*). Recently published structural and biochemical data indicate that N-CAP also forms a dimer (*36*). Moreover, biochemical isolation of mammalian CAP from porcine platelets (*7*), HEK293 cells (*21*), and *S. cerevisiae* (*37*) reveals that CAP and actin form a high-molecular weight complex containing multiple actin and CAP molecules. The current structural and biochemical observations, including the dimeric properties and binding activities of N-CAP and C-CAP, the placement of the C-CAP N-terminus, and the likely binding of C-CAP in the vicinity of actin subdomains 1 and 3, all provide significant constraints for the organization of the actin−CAP assembly and the mechanisms by which it regulates actin filament dynamics.

The quaternary features of CAP also impact the function of a wide range of actin regulatory proteins involved in actin filament nucleation, severing, and localization. In yeast, CAP and ABP1 colocalize to cortical actin patches, which are centers of active actin polymerization that target sites of polarized cell growth (*6*, *10*). These proteins also appear to

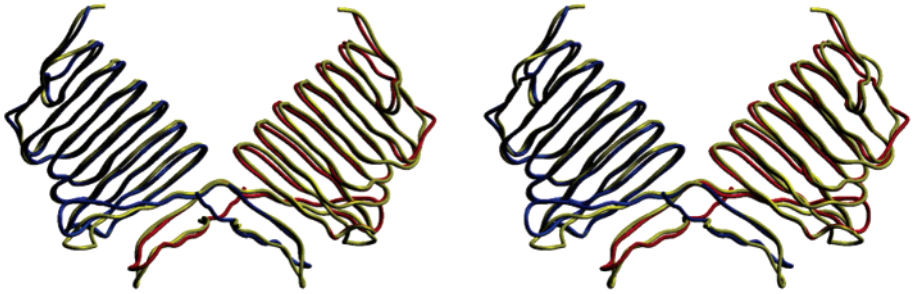

FIGURE 6: Superposition of the *S. cerevisiae* (yellow) and human (red and blue) C-CAP domains. Superposition of all backbone atoms yields an rms deviation of 0.6 Å.

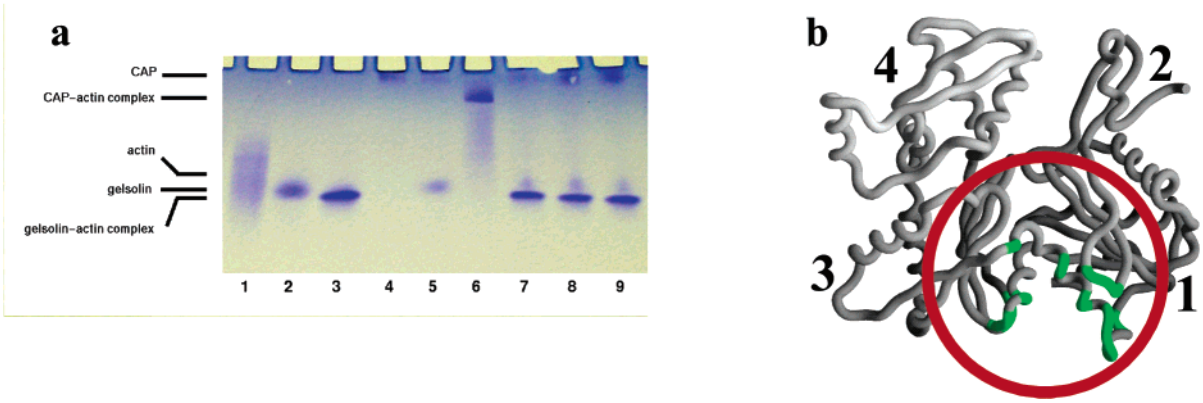

FIGURE 7: Interaction between CAP and G-actin. (a) Native polyacrylamide gel analysis demonstrates that gelsolin competes with CAP *in vitro*: lane 1, actin; lane 2, gelsolin S1 domain; lane 3, gelsolin−actin complex (24 and 16 μM, respectively); lane 4, CAP; lane 5, CAP and gelsolin (10 and 24 μM, respectively) showing no interaction; lane 6, CAP−actin complex (24 and 24 μM, respectively). Competition between CAP and gelsolin for G-actin is demonstrated in lanes 7−9, which contain 1:1.5:1.3, 1:1.5:2.0, and 1:1.5:2.3 G-actin:gelsolin:CAP stoichiometries, respectively. (b) Potential G-actin binding site for CAP. Residues in subdomains 1 and 3 of G-actin that bind gelsolin S1 are highlighted in green. On the basis of the direct competition between CAP and S1, the region encircled in red represents a potential C-CAP binding surface for G-actin.

be involved in dynamic cytoskeletal events in mammalian systems, as the mammalian homologues of CAP and ABP1 accumulate in the lamellipodia of motile cells. Furthermore, ABP1 has been shown to localize to sites enriched in the Arp2/3 complex, the major engine for *de novo* nucleation of actin filaments (*15*, *38*). This latter observation is particularly striking, as recent reports have demonstrated that ABP1 can serve as a direct activator of Arp2/3-catalyzed filament nucleation (*39*). In addition, recent structural analysis of the N-terminal cofilin homology domain of ABP1 suggests that under appropriate circumstances ABP1 may exist as a dimer (Strokopytov and S. C. Almo, unpublished data), further adding to the geometric and organizational complexity of the assemblies associated with CAP function. The functional interaction between CAP, ABP1, and Arp2/3 suggests the possibility of a multicomponent F-actin nucleating assembly that could provide a link to SH3-mediated signaling pathways. Furthermore, in addition to the specific ABP1-mediated activation of Arp2/3, the G- and F-actin binding activities of CAP and ABP1, respectively, suggest additional levels of Arp2/3 modulation. This situation is further enriched by biochemical linkage of CAP and filament severing protein cofilin, as well as the recently described two-hybrid interaction between CAP and Aip1 (*40*), a protein that modulates cofilin-mediated actin filament severing by capping and preventing annealing of severed ends. Thus, the emerging structural analyses are beginning to define the organizational principles that direct the structural, biochemical, and mechanistic features of the multicomponent assemblies that integrate Arp2/3 function into the overall physiology of the cell.

Topological Comparison to Other Members of the Right-Handed β-Helical Family. A number of parallel β-helix family members have been reported, including pectate lyase (*27*), pectin methylesterase (*29*), the tail spike protein of phage P22 (*41*), the IGF-1R domain (*42*), the bacterial cell division inhibitor MinC (*43*), chondroitinase B (*44*), pertactin (*45*), galacturonase (*46*, *47*), alkaline protease (*48*, *49*), and the TmAFP antifreeze protein (*50*). In contrast to the elliptical, almost rectangular C-CAP, the majority of these structures display "L-shaped" cross sections (Figure 3). The alkaline protease and TmAFP antifreeze protein are the only other family members that exhibit nearly elliptical cross sections; however, the detailed disposition of strands within their β-helices differs significantly from that observed in C-CAP. The alkaline protease β-helix has only the equivalent of β-sheets PB1 and PB2, which are nearly antiparallel to each other. In C-CAP, the additional β-sheet PB1a runs approximately perpendicular to both PB1 and PB2. The TmAFP antifreeze protein exhibits the smallest β-helix with only 12 residues per helical coil. Like C-CAP, TmAFP contains nearly perpendicular β-sheets PB1 and PB1a; however, it lacks sheet PB2, which is replaced by a short loop that connects PB1a with the next coil. Galacturonase, despite its L-shaped cross section, is the right-handed β-helix most similar to C-CAP, as both structures have β-sheet PB1a, nearly perpendicular to sheets PB1 and PB2, and in both structures, all strands in β-sheet PB1a consist of two residues.

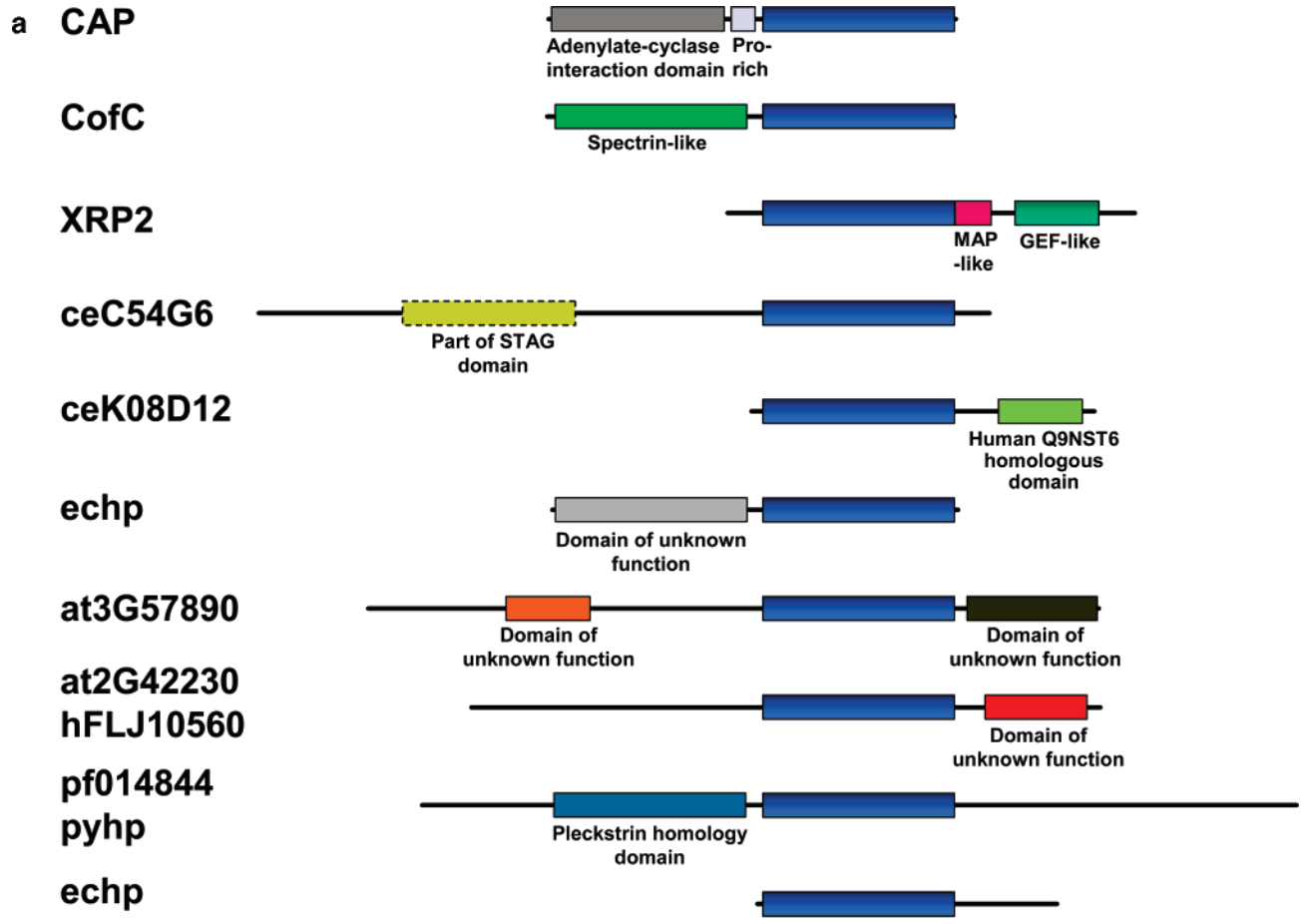
a
CAP
Adenylate-cyclase interaction domain
Pro-rich
CofC
Spectrin-like
XRP2
MAP -like
GEF-like
ceC54G6
Part of STAG domain
ceK08D12
Human Q9NST6 homologous domain
echp
Domain of unknown function
at3G57890
Domain of unknown function
Domain of unknown function
at2G42230
hFLJ10560
Domain of unknown function
pf014844
pyhp
Pleckstrin homology domain
echp

b

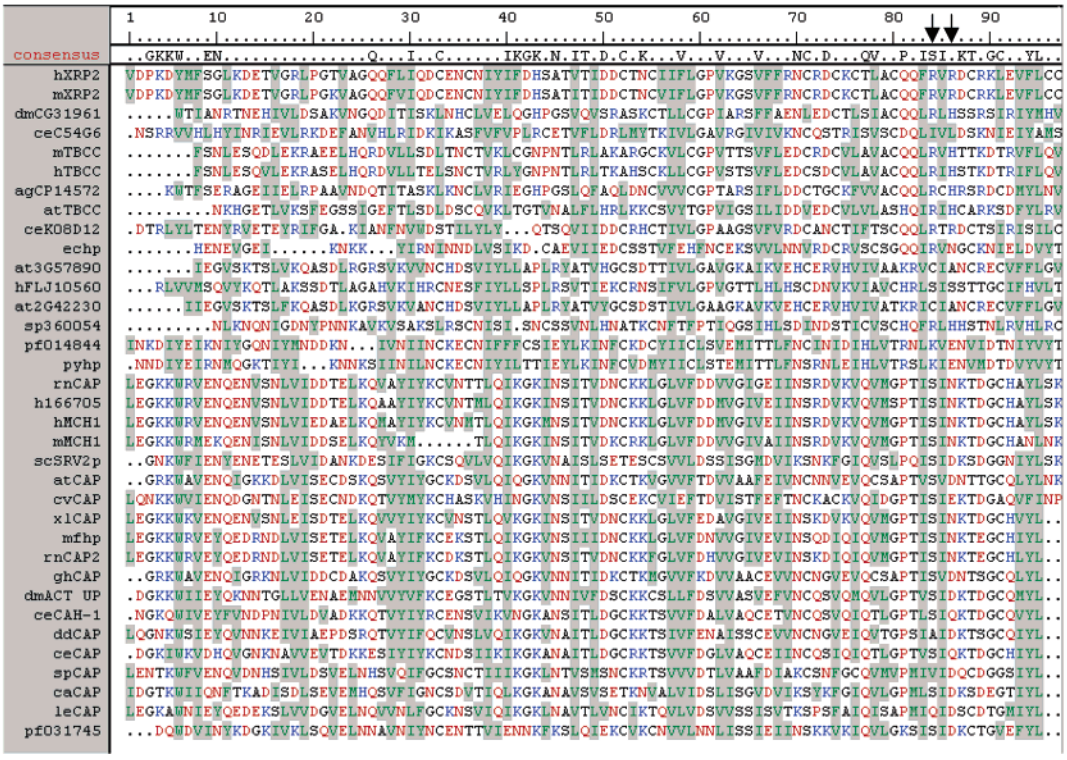
consensus
hXRP2
mXRP2
dmCG31961
ceC54G6
mTBCC
hTBCC
agCP14572
atTBCC
ceK08D12
echp
at3G57890
hFLJ10560
at2G42230
sp360054
pf014844
pyhp
rnCAP
h166705
hMCH1
mMCH1
scSRV2p
atCAP
cvCAP
xlCAP
mfhp
rnCAP2
ghCAP
dmACT UP
ceCAH-1
ddCAP
ceCAP
spCAP
caCAP
leCAP
pf031745

FIGURE 8: (a) Extended C-CAP family domain architecture. The C-CAP domain is shown in blue. The names (left part of the figure) correspond to sequences below. (b) Amino acid sequence alignment of the C-CAP/RP2/cofactor C family. The shaded residues represent the identical/similar positions, whereas red and blue indicate the hydrophobicity code. The black arrows indicate the positions of two solvent accessible disease-related mutations in the RP2 model. Abbreviations (numbers represent the GenBank entries; numbers in brackets denote the region of similarity): hXRP2, human 5902060 (35−131); mXRP2, mouse 19526820 (32−128); dmCG31961, *Drosophila melanogaster* 16198141 (169−260); ceC54G6, *Caenorhabditis elegans* 17506233 (542−640); mTBCC, mouse 20900199 (181−270); hTBCC, human 4507373 (186−275); agCP14572, *Anopheles gambiae* 21293700 (186−277); atTBCC, *Arabidopsis thaliana* 20514261 (178−265); ceK08D12, *C. elegans* 17541340 (80−171); echp, *Encephalitozoon cuniculi* 19173507 (98−177); at3G57890, *A. thaliana* 18410836 (320−409); hFLJ10560, human 8922517 (308−401); at2G42230, *A. thaliana* 15227909 (262−352); sp360054, *Schizosaccharomyces pombe* 19115122 (125−214); pf014844, *Plasmodium falciparum* 23508730 (526−619); pyhp, *Plasmodium yoelii yoelii* 23480834 (440−532); rnCAP, rat 11693146 (323−421); h166705, human 22053238 (113-211); hMCH1, human 18555162 (47−145); mMCH1, mouse 20872780 (95−187); scSRV2p, *S. cerevisiae* 6324191 (376−472); atCAP, *A. thaliana* 15236128 (324−420); cvCAP, *Chlorohydra viridissima* 729031 (328−426); xlCAP, *Xenopus laevis* 17222946 (324−420); mfhp, *Macaca fascicularis* 13874486 (251−347); rnCAP2, rat 16758742 (327−423); ghCAP, *Gossypium hirsutum* 4126473 (320−414); dmACT UP, *D. melanogaster* 17864428 (274−369); ceCAH-1, *C. elegans* 17551210 (1106−1201); ddCAP, *D. discoideum* 1705592 (312−408); ceCAP, *C. elegans* 17505663 (306−401); spCAP, *S. pombe* 19075317 (400−496); caCAP, *Candida albicans* 5381432 (388−488); leCAP, *Lentinula edodes* 3126641 (364−460); pf031745, *P. falciparum* 23613411 (12−106). The alignment and editing were prepared using the Octopus program (*59*).

The major difference between these two structures is the presence of the additional fourth β-sheet PB3, and an additional residue in the α_L conformation that connects PB2 and PB3 in galacturonase.

Evolutionary Relations. Detailed sequence analysis suggests that the C-CAP β-helical core may represent the structural archetype for a wide range of biologically diverse proteins (Figure 8). More than 30 proteins that are homologous over a span of approximately 100 amino acids were identified. Two subfamilies, which are characterized by their sequences and domain architecture, account for the majority of the homologues. Several uncharacterized proteins from plants, animals, and lower eukaryotes with diverse domain architectures account for the remaining homologues (Figure 8).

The most intriguing homology is that between C-CAP and the C-terminal domain of cofactor C (~90 amino acids), a GTPase-activating component of the tubulin-folding supercomplex (*51*, *52*), which directs the assembly of the α- and β-tubulin heterodimer (Figure 8). This same domain is also present in the N-terminus of RP2, the protein responsible for X-linked forms of *retinitis pigmentosa*, a disease characterized by severe retinal degeneration (*53*). Remarkably, the homology model of RP2 and the experimental C-CAP structures exhibit the same "internal Ser/Cys stack" in the first position of the b strands that form the PB1a sheet, which supports the validity of the RP2 model (Figure 9). Importantly, a significant fraction of the clinically relevant RP2 mutations are located in the C-CAP/cofactor C-like domain, and the RP2 model allows a number of the disease-associated mutations to be rationalized. Several insertion and/or deletion mutations, such as the 13 bp insertion at Cys110, the 2 bp insertion at Phe117, and the 1 bp insertion at Arg123, result not only in frame shifts but also in premature terminations, likely resulting in the production of nonfunctional polypeptides (*54*−*56*). A 3 bp deletion at Ile137 preserves the reading frame, but results in the removal of a single amino acid in the middle of a strand that contributes to the putative PB1 sheet, and likely results in global destabilization (*53*, *55*, *57*). A point mutation at Arg120 directs premature termination, which would effectively remove the last coils of the putative RP2 β-helix (*56*), exposing the hydrophobic core to solvent, and thus yield a defective polypeptide that is unable to fold properly. Independent point mutations involving the alteration of Cys67 and Cys86 to Tyr are predicted to result in a defective protein due to the imposition of a large bulky

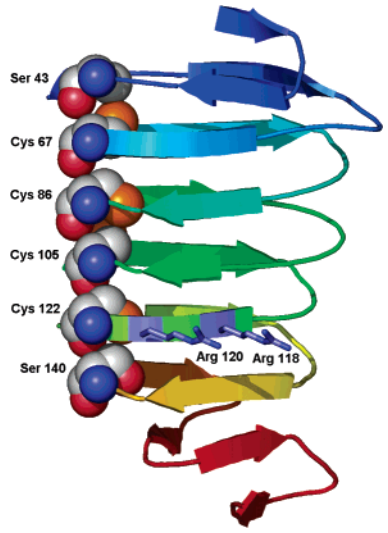

FIGURE 9: Homology model of RP2. The homology model of RP2 exhibits the same basic β-helical motif present in the yeast and human C-CAP molecules. The internal Cys/Ser ladder, which is shared by RP2 and C-CAP, is highlighted in a space filling representation (sulfur shaded orange). Cys67 and Cys86 are the locations of naturally occurring disease-related mutations. Arg118 and Arg120 are solvent accessible residues that have also been implicated in the disease state.

aromatic residue at highly conserved positions of the "internal Ser/Cys stack" which contributes to the hydrophobic core of RP2. The Cys108Gly mutation may result in a destabilized protein due the introduction of a "hole" in the middle of the tightly packed RP2 hydrophobic core.

The homology observed between cofactor C and RP2 might have functional significance as this domain in RP2 has recently been suggested to play a role in tubulin biology (*54*). RP2, apart from having the C-CAP/cofactor C-like domain, possesses both a microtubule-associated-like domain (MAP-like) and a guanine exchange factor-related domain (GEF-related), both of which are involved in microtubule biogenesis (*54*). Recent studies have shown that both cofactor C and RP2 stimulate the GTPase activity of tubulin (*58*). Moreover, this activity is abolished in both proteins by mutation of the equivalent of Arg118 in RP2, which is highly conserved in RP2 and cofactor C. Importantly, the naturally occurring Arg118His (*53*, *55*, *57*) and Arg118Leu (*54*) point mutations in RP2 are correlated with the disease state. This residue is thought to function in a manner analogous to that of the "arginine fingers" present in GTPase activating proteins (GAPs) to trigger the GTPase activity of tubulin

(*58*), suggesting that the defect associated with this mutant is due to the loss of essential function and not a consequence of compromised protein structure or stability. While the equivalent of Arg118 is not conserved throughout the entire extended family, variation at this position is clearly restricted and does not exist within subfamilies, suggesting that C-CAP homologues bind to a small number of well-defined targets. It is notable that the C-CAP/cofactor C-like domain is present in several other uncharacterized proteins, which also contain a number of additional domains, suggesting that many signaling pathways utilize this cytoskeleton-related motif.

SUMMARY

The C-terminal oligomerization and G-actin binding domain of the cyclase-associated protein (C−CAP) is a new member of the right-handed β-helical superfamily. An intimate parallel dimer is formed by domain swapping, involving the exchange of the two C-terminal β-strands. These structural features, in combination with the biochemical properties of C-CAP, place significant constraints on the organizational, mechanistic, and regulatory features relevant to CAP function. Moreover, the unique β-helical core observed in C-CAP provides a useful structural model for functional domains found across a wide range of proteins with relatively modest levels of sequence homology, including RP2 and cofactor C, the proteins involved in X-linked *retinitis pigmentosa* and the maturation of tubulin, respectively.

ACKNOWLEDGMENT

We thank Takahiro Morio for providing the *Dictyostelium* CAP cDNA. We thank Dr. Zbignew Dauter for his assistance with data collection at beamline X9B.

REFERENCES

1. Field, J., Vojtek, A., Ballester, R., Bolger, G., Colicelli, J., Ferguson, K., Gerst, J., Kataoka, T., Michaeli, T., Powers, S., et al. (1990) Cloning and characterization of CAP, the *S. cerevisiae* gene encoding the 70 kd adenylyl cyclase-associated protein, *Cell 61*, 319−327.
2. Fedor-Chaiken, M., Deschenes, R. J., and Broach, J. R. (1990) SRV2, a gene required for RAS activation of adenylate cyclase in yeast, *Cell 61*, 329−340.
3. Vojtek, A., Haarer, B., Field, J., Gerst, J., Pollard, T. D., Brown, S., and Wigler, M. (1991) Evidence for a functional link between profilin and CAP in the yeast *S. cerevisiae*, *Cell 66*, 497−505.
4. Mintzer, K. A., and Field, J. (1994) Interactions between adenylyl cyclase, CAP and RAS from *Saccharomyces cerevisiae*, *Cell. Signalling 6*, 681−694.
5. Gerst, J. E., Ferguson, K., Vojtek, A., Wigler, M., and Field, J. (1991) CAP is a bifunctional component of the *Saccharomyces cerevisiae* adenylyl cyclase complex, *Mol. Cell. Biol. 11*, 1248−1257.
6. Freeman, N. L., Lila, T., Mintzer, K. A., Chen, Z., Pahk, A. J., Ren, R., Drubin, D. G., and Field, J. (1996) A conserved proline-rich region of the *Saccharomyces cerevisiae* cyclase-associated protein binds SH3 domains and modulates cytoskeletal localization, *Mol. Cell. Biol. 16*, 548−556.
7. Gieselmann, R., and Mann, K. (1992) ASP-56, a new actin sequestering protein from pig platelets with homology to CAP, an adenylate cyclase-associated protein from yeast, *FEBS Lett. 298*, 149−153.
8. Gottwald, U., Brokamp, R., Karakesisoglou, I., Schleicher, M., and Noegel, A. A. (1996) Identification of a cyclase-associated protein (CAP) homologue in *Dictyostelium discoideum* and characterization of its interaction with actin, *Mol. Biol. Cell 7*, 261−272.
9. Zelicof, A., Protopopov, V., David, D., Lin, X. Y., Lustgarten, V., and Gerst, J. E. (1996) Two separate functions are encoded by the carboxyl-terminal domains of the yeast cyclase-associated protein and its mammalian homologues. Dimerization and actin binding, *J. Biol. Chem. 271*, 18243−18252.
10. Lila, T., and Drubin, D. G. (1997) Evidence for physical and functional interactions among two *Saccharomyces cerevisiae* SH3 domain proteins, an adenylyl cyclase-associated protein and the actin cytoskeleton, *Mol. Biol. Cell 8*, 367−385.
11. Yu, J., Wang, C., Palmieri, S. J., Haarer, B. K., and Field, J. (1999) A cytoskeletal localizing domain in the cyclase-associated protein, CAP/Srv2p, regulates access to a distant SH3-binding site, *J. Biol. Chem. 274*, 19985−19991.
12. Noegel, A. A., Rivero, F., Albrecht, R., Janssen, K. P., Kohler, J., Parent, C. A., and Schleicher, M. (1999) Assessing the role of the ASP56/CAP homologue of *Dictyostelium discoideum* and the requirements for subcellular localization, *J. Cell Sci. 112*, 3195−3203.
13. Kawamukai, M., Gerst, J., Field, J., Riggs, M., Rodgers, L., Wigler, M., and Young, D. (1992) Genetic and biochemical analysis of the adenylyl cyclase-associated protein, cap, in *Schizosaccharomyces pombe*, *Mol. Biol. Cell 3*, 167−180.
14. Zhou, G. L., Miyazaki, Y., Nakagawa, T., Tanaka, K., Shishido, K., Matsuda, H., and Kawamukai, M. (1998) Identification of a CAP (adenylyl-cyclase-associated protein) homologous gene in *Lentinus edodes* and its functional complementation of yeast CAP mutants, *Microbiology 144*, 1085−1093.
15. Vojtek, A. B., and Cooper, J. A. (1993) Identification and characterization of a cDNA encoding mouse CAP: a homolog of the yeast adenylyl cyclase associated protein, *J. Cell Sci. 105*, 777−785.
16. Matviw, H., Yu, G., and Young, D. (1992) Identification of a human cDNA encoding a protein that is structurally and functionally related to the yeast adenylyl cyclase-associated CAP proteins, *Mol. Cell. Biol. 12*, 5033−5040.
17. Stevenson, V. A., and Theurkauf, W. E. (2000) Actin cytoskeleton: putting a CAP on actin polymerization, *Curr. Biol. 10*, R695−R697.
18. Baum, B., Li, W., and Perrimon, N. (2000) A cyclase-associated protein regulates actin and cell polarity during *Drosophila* oogenesis and in yeast, *Curr. Biol. 10*, 964−973.
19. Baum, B., and Perrimon, N. (2001) Spatial control of the actin cytoskeleton in *Drosophila* epithelial cells, *Nat. Cell Biol. 3*, 883−890.
20. Freeman, N. L., and Field, J. (2000) Mammalian homolog of the yeast cyclase associated protein, CAP/Srv2p, regulates actin filament assembly, *Cell Motil. Cytoskeleton 45*, 106−120.
21. Moriyama, K., and Yahara, I. (2002) Human CAP1 is a key factor in the recycling of cofilin and actin for rapid actin turnover, *J. Cell Sci. 115*, 1591−1601.
22. Collaborative Computational Project No. 4 (1994) *Acta Crystallogr. D50*, 760−763.
23. Otwinowski, Z., and Minor, W. (1997) Processing of X-ray diffraction data collected in oscillation mode, *Methods Enzymol. 276*, 307−326.
24. Terwilliger, T. C., and Berendzen, J. (1999) Automated MAD and MIR structure solution, *Acta Crystallogr. D55*, 849−861.
25. Brünger, A. T. (1992) *X-PLOR*, version 3.1, Yale Universtiy Press, New Haven, CT.
26. Laskowski, R. A., MacArthur, M. W., Moss, D. S., and Thornton, J. M. (1993) PROCHECK: a program to check the stereochemical quality of protein structures, *J. Appl. Crystallogr.*, 283−291.
27. Yoder, M. D., Keen, N. T., and Jurnak, F. (1993) New domain motif: the structure of pectate lyase C, a secreted plant virulence factor, *Science 260*, 1503−1507.
28. Yoder, M. D., Lietzke, S. E., and Jurnak, F. (1993) Unusual structural features in the parallel β-helix in pectate lyases, *Structure 1*, 241−251.
29. Jenkins, J., Mayans, O., Smith, D., Worboys, K., and Pickersgill, R. W. (2001) Three-dimensional structure of *Erwinia chrysanthemi* pectin methylesterase reveals a novel esterase active site, *J. Mol. Biol. 305*, 951−960.
30. McLaughlin, P. J., Gooch, J. T., Mannherz, H. G., and Weeds, A. G. (1993) Structure of gelsolin segment 1-actin complex and the mechanism of filament severing, *Nature 364*, 685−692.
31. Altschul, S. F., Madden, T. L., Schaffer, A. A., Zhang, J., Zhang, Z., Miller, W., and Lipman, D. J. (1997) Gapped BLAST and PSI-BLAST: a new generation of protein database search programs, *Nucleic Acids Res. 25*, 3389−3402.

32. Li, W., Pio, F., Pawlowski, K., and Godzik, A. (2000) Saturated BLAST: an automated multiple intermediate sequence search used to detect distant homology, *Bioinformatics 16*, 1105−1110.
33. Rychlewski, L., Jaroszewski, L., Li, W., and Godzik, A. (2000) Comparison of sequence profiles. Strategies for structural predictions using sequence information, *Protein Sci. 9*, 232−241.
34. Hubberstey, A. V., and Mottillo, E. P. (2002) Cyclase-associated proteins: CAPacity for linking signal transduction and actin polymerization, *FASEB J. 16*, 487−499.
35. Freeman, N. L., Chen, Z., Horenstein, J., Weber, A., and Field, J. (1995) An actin monomer binding activity localizes to the carboxyl-terminal half of the *Saccharomyces cerevisiae* cyclase-associated protein, *J. Biol. Chem. 270*, 5680−5685.
36. Ksiazek, D., Brandstetter, H., Israel, L., Bourenkov, G. P., Katchalova, G., Janssen, K. P., Bartunik, H. D., Noegel, A. A., Schleicher, M., and Holak, T. A. (2003) Structure of the N-terminal domain of the adenylyl cyclase-associated protein (CAP) from *Dictyostelium discoideum*, *Structure 11*, 1171−1178.
37. Balcer, H. I., Goodman, A. L., Rodal, A. A., Smith, E., Kugler, J., Heuser, J. E., and Goode, B. L. (2003) Coordinated regulation of actin filament turnover by a high-molecular-weight Srv2/CAP complex, cofilin, profilin, and Aip1, *Curr. Biol. 13*, 2159−2169.
38. Kessels, M. M., Engqvist-Goldstein, A. E., and Drubin, D. G. (2000) Association of mouse actin-binding protein 1 (mAbp1/SH3P7), an Src kinase target, with dynamic regions of the cortical actin cytoskeleton in response to Rac1 activation, *Mol. Biol. Cell 11*, 393−412.
39. Goode, B. L., Rodal, A. A., Barnes, G., and Drubin, D. G. (2001) Activation of the Arp2/3 complex by the actin filament binding protein Abp1p, *J. Cell Biol. 153*, 627−634.
40. Drees, B. L., Sundin, B., Brazeau, E., Caviston, J. P., Chen, G. C., Guo, W., Kozminski, K. G., Lau, M. W., Moskow, J. J., Tong, A., Schenkman, L. R., McKenzie, A., III, Brennwald, P., Longtine, M., Bi, E., Chan, C., Novick, P., Boone, C., Pringle, J. R., Davis, T. N., Fields, S., and Drubin, D. G. (2001) A protein interaction map for cell polarity development, *J. Cell Biol. 154*, 549−571.
41. Steinbacher, S., Baxa, U., Miller, S., Weintraub, A., Seckler, R., and Huber, R. (1996) Crystal structure of phage P22 tailspike protein complexed with *Salmonella* sp. O-antigen receptors, *Proc. Natl. Acad. Sci. U.S.A. 93*, 10584−10588.
42. Garrett, T. P., McKern, N. M., Lou, M., Frenkel, M. J., Bentley, J. D., Lovrecz, G. O., Elleman, T. C., Cosgrove, L. J., and Ward, C. W. (1998) Crystal structure of the first three domains of the type-1 insulin-like growth factor receptor, *Nature 394*, 395−399.
43. Cordell, S. C., Anderson, R. E., and Lowe, J. (2001) Crystal structure of the bacterial cell division inhibitor MinC, *EMBO J. 20*, 2454−2461.
44. Huang, W., Matte, A., Li, Y., Kim, Y. S., Linhardt, R. J., Su, H., and Cygler, M. (1999) Crystal structure of chondroitinase B from *Flavobacterium heparinum* and its complex with a disaccharide product at 1.7 Å resolution, *J. Mol. Biol. 294*, 1257−1269.
45. Emsley, P., Charles, I. G., Fairweather, N. F., and Isaacs, N. W. (1996) Structure of *Bordetella pertussis* virulence factor P.69 pertactin, *Nature 381*, 90−92.
46. van Santen, Y., Benen, J. A., Schroter, K. H., Kalk, K. H., Armand, S., Visser, J., and Dijkstra, B. W. (1999) 1.68-Å crystal structure of endopolygalacturonase II from *Aspergillus niger* and identification of active site residues by site-directed mutagenesis, *J. Biol. Chem. 274*, 30474−30480.
47. Pickersgill, R., Smith, D., Worboys, K., and Jenkins, J. (1998) Crystal structure of polygalacturonase from *Erwinia carotovora* ssp. *carotovora*, *J. Biol. Chem. 273*, 24660−24664.
48. Miyatake, H., Hata, Y., Fujii, T., Hamada, K., Morihara, K., and Katsube, Y. (1995) Crystal structure of the unliganded alkaline protease from *Pseudomonas aeruginosa* IFO3080 and its conformational changes on ligand binding, *J. Biochem. 118*, 474−479.
49. Hamada, K., Hata, Y., Katsuya, Y., Hiramatsu, H., Fujiwara, T., and Katsube, Y. (1996) Crystal structure of *Serratia protease*, a zinc-dependent proteinase from *Serratia* sp. E-15, containing a β-sheet coil motif at 2.0 Å resolution, *J. Biochem. 119*, 844−851.
50. Graether, S. P., Kuiper, M. J., Gagne, S. M., Walker, V. K., Jia, Z., Sykes, B. D., and Davies, P. L. (2000) β-Helix structure and ice-binding properties of a hyperactive antifreeze protein from an insect, *Nature 406*, 325−328.
51. Cowan, N. J., and Lewis, S. A. (1999) A chaperone with a hydrophilic surface, *Nat. Struct. Biol. 6*, 990−991.
52. Tian, G., Bhamidipati, A., Cowan, N. J., and Lewis, S. A. (1999) Tubulin folding cofactors as GTPase-activating proteins. GTP hydrolysis and the assembly of the α/β-tubulin heterodimer, *J. Biol. Chem. 274*, 24054−24058.
53. Schwahn, U., Lenzner, S., Dong, J., Feil, S., Hinzmann, B., van Duijnhoven, G., Kirschner, R., Hemberger, M., Bergen, A. A., Rosenberg, T., Pinckers, A. J., Fundele, R., Rosenthal, A., Cremers, F. P., Ropers, H. H., and Berger, W. (1998) Positional cloning of the gene for X-linked retinitis pigmentosa 2, *Nat. Genet. 19*, 327−332.
54. Miano, M. G., Testa, F., Filippini, F., Trujillo, M., Conte, I., Lanzara, C., Millan, J. M., De Bernardo, C., Grammatico, B., Mangino, M., Torrente, I., Carrozzo, R., Simonelli, F., Rinaldi, E., Ventruto, V., D'Urso, M., Ayuso, C., and Ciccodicola, A. (2001) Identification of novel RP2 mutations in a subset of X-linked retinitis pigmentosa families and prediction of new domains, *Hum. Mutat. 18*, 109−119.
55. Breuer, D. K., Yashar, B. M., Filippova, E., Hiriyanna, S., Lyons, R. H., Mears, A. J., Asaye, B., Acar, C., Vervoort, R., Wright, A. F., Musarella, M. A., Wheeler, P., MacDonald, I., Iannaccone, A., Birch, D., Hoffman, D. R., Fishman, G. A., Heckenlively, J. R., Jacobson, S. G., Sieving, P. A., and Swaroop, A. (2002) A comprehensive mutation analysis of RP2 and RPGR in a North American cohort of families with X-linked retinitis pigmentosa, *Am. J. Hum. Genet. 70*, 1545−1554.
56. Mears, A. J., Gieser, L., Yan, D., Chen, C., Fahrner, S., Hiriyanna, S., Fujita, R., Jacobson, S. G., Sieving, P. A., and Swaroop, A. (1999) Protein-truncation mutations in the RP2 gene in a North American cohort of families with X-linked retinitis pigmentosa, *Am. J. Hum. Genet. 64*, 897−900.
57. Sharon, D., Bruns, G. A., McGee, T. L., Sandberg, M. A., Berson, E. L., and Dryja, T. P. (2000) X-linked retinitis pigmentosa: mutation spectrum of the RPGR and RP2 genes and correlation with visual function, *Invest. Ophthalmol. Visual Sci. 41*, 2712−2721.
58. Bartolini, F., Bhamidipati, A., Thomas, S., Schwahn, U., Lewis, S. A., and Cowan, N. J. (2002) Functional overlap between retinitis pigmentosa 2 protein and the tubulin-specific chaperone cofactor C, *J. Biol. Chem. 277*, 14629−14634.
59. Durand, P., Canard, L., and Mornon, J. P. (1997) Visual BLAST and visual FASTA: graphic workbenches for interactive analysis of full BLAST and FASTA outputs under MICROSOFT WINDOWS 95/NT, *Comput. Appl. Biosci. 13*, 407−413.
60. Philips, W. C., et al. (2001) High Sensitivity CCD-based X-ray detector, *J. Synchrotron Radiat. 9*, 36−43.

BI049071R